# X-RAY MICROBEAM MEASUREMENT OF LOCAL TEXTURE AND STRAIN IN METALS

Jin-Seok Chung, N. Tamura, G. E. Ice, B. C. Larson, J. D. Budai, Oak Ridge National Laboratory, Oak Ridge, TN, Walter Lowe, Howard University, Washington D.C.

## ABSTRACT

Synchrotron x-ray sources provide high-brilliance beams that can be focused to submicron sizes with Fresnel zone-plate and x-ray mirror optics. With these intense, tunable or broad-bandpass x-ray microbeams, it is now possible to study texture and strain distributions in surfaces, and in buried or encapsulated thin films. The full strain tensor and local texture can be determined by measuring the unit cell parameters of strained material. With monochromatic or tunable radiation, at least three independent reflections are needed to determine the orientation and unit cell parameters of an unknown crystal. With broad-bandpass or white radiation, at least four reflections and one measured energy are required to determine the orientation and the unit cell parameters of an unknown crystal. Routine measurement of local texture and strain is made possible by automatic indexing of the Laue reflections combined with precision calibration of the monochromator-focusing mirrors-CCD detector system. Methods used in implementing these techniques on the MHATT-CAT beam line at the Advanced Photon Source will be discussed.

## INTRODUCTION

Material science has traditionally concentrated on studies either at the atomic scale where first principles and Monte-Carlo simulations are practical or at the macroscopic scale where finite element methods are appropriate. However at an intermediate mesoscale (of order 10nm to 10μm), both theoretical and experimental tools are limited. Yet it is just at this scale where polycrystalline and intra-granular heterogeneities support a rich system of boundaries, stress distributions, second phases and interfaces, which are keys to understand fundamental material behaviors.

Electron backscatter diffraction (EBSD) is one of the few tools which can be used to study crystal structure at mesoscopic length scales[1]. However, electron beam probes are limited to the near-surface region and typically have limited strain and texture sensitivity. Penetrating x-ray microprobes overcome both limitations with strain sensitivity down to $\Delta d / d \sim 10^{-4}$. X-ray microbeams also have outstanding elemental and oxidation state sensitivity with probe sizes comparable to electron beams on thick samples. Yet despite the many advantages of x-ray microprobes, these devices have been largely limited by x-ray brilliance (photons/sec/eV/mm$^2$/mrad$^2$).

The recent availability of the third generation synchrotron radiation sources like the Advanced Photon Source at Argonne National Laboratory now provides orders of magnitude greater brilliance in the hard x-ray region. Third generation sources combined with much improved x-ray optical components like elliptic Kirkpatrick-Baez mirrors and Fresnel zone plates can provide submicron size focused x-ray beams which have more flux than mm$^2$ beams from a conventional x-ray tube. X-ray microprobes can now be used for local texture and strain analysis on a micron scale. Of particular interest are studies of inter- and intra-granular stress/strain distributions in polycrystalline samples.

$$\mathbf{A_M}\ \mathbf{v} = \mathbf{T}\,\mathbf{A_0}\,\mathbf{v} \qquad (2)$$

$$\mathbf{T} = \mathbf{A_M}\,\mathbf{A_0}^{-1} \qquad (3)$$

The transformation matrix **T** can be calculated from the measured lattice parameters with Eq. (1). But **T** may include both distortions and rotations. To remove the rotations, the average of **T** and $\mathbf{T}^T$ must be used. The strain tensor $\varepsilon_M$ in the measured crystal Cartesian coordinates is given by,

$$\varepsilon_M = (\mathbf{T} + \mathbf{T}^T) / 2 - \mathbf{I} \qquad (4)$$

where **I** is the identity matrix. The strain tensor in a laboratory frame, $\varepsilon_L$ can be calculated by using the rotation matrix **R**, which is derived from the orientation of the grain;

$$\varepsilon_L = \mathbf{R}\,\varepsilon_M\,\mathbf{R}^{-1}. \qquad (5)$$

This simple method allows the calculation of the strain tensor for each grain from the measured unit cell parameters. We note that the strain tensor can be divided into a dilatation tensor and a deviatoric tensor[5]. For some cases, the distortional tensor alone is adequate, and this can be recovered from a white beam Laue pattern alone without energy measurements of the diffracted beams.

## EXPERIMENT

A schematic diagram of the setup used at the MHATT-CAT 7ID-beam line at the APS is shown in Fig. 1. Absolute values of lattice constants could be obtained by switching back and forth between white beam and monochromatic beam. Whereas a typical monochromator has large displacements on the order of cm's between the white beam and the monochromatic beam, for the x-ray microbeam experiments, both beams need to illuminate the same spot on the sample. To achieve this goal, a monochromator was specially designed so that the monochromatic beam direction can be adjusted to make it co-axial to the white beam[6]. The geometry of slits and monochromator crystals is also shown in Fig. 1.

To focus the x-ray beam down to a submicron size, a pair of Kirkpatrick-Baez mirrors was

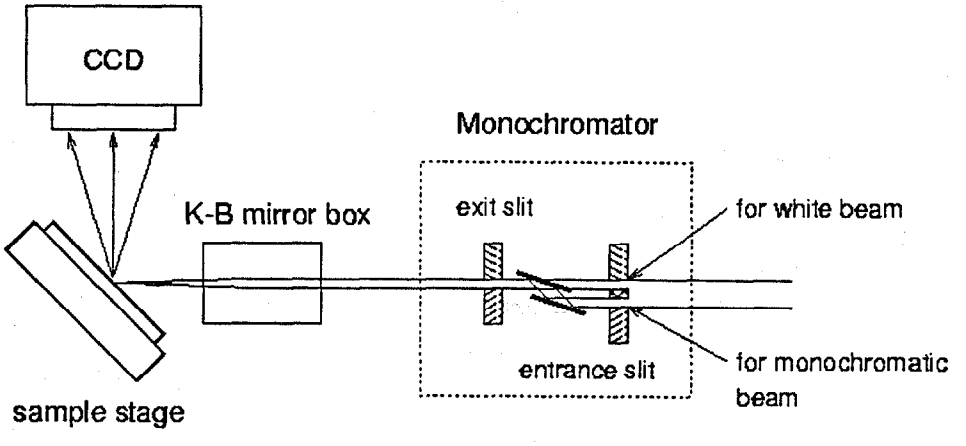


Figure 1. A schematic diagram of the x-ray microbeam experiment. For the white beam, crystals are placed out of the path and only the top part of the entrance slit is open. For the monochromatic beam, only the bottom entrance slit is open and the monochromator crystals are placed in the beam path.

used. A gold film was differentially deposited on a pair of Si cylindrical mirrors to achieve an elliptic shape and a Rhodium film was coated on top to improve the reflectivity. The nominal size of the focused beam is 0.7μm x 0.7μm for both the white and the monochromatic beam. As shown in Fig. 1, the monochromatic beam comes from a region about 1mm below the white beam. Therefore, the vertical angle of the monochromatic beam is slightly different from the white beam. To make the monochromatic beam illuminate the same part of the sample, the beam direction is adjusted by raising the temperature of the second crystal of the monochromator. The positions of both beams at the focus were adjusted to within ~0.5 μm from each other.

Reflections from the sample were recorded with a thermoelectrically cooled CCD with 1242 by 1152 pixels from Princeton Instruments Inc. Though its pixel size is ~22.5 μm, the position of a peak can be determined to ~1/10 of the pixel size by fitting the curve shape of the intensity profile. Each pixel has 16 bits of the dynamic range.

To measure a strain tensor to $10^{-4}$ resolution, the angles of the diffracted beams have to be measured very accurately. An accurate determination of a CCD detector orientation relative to the x-ray beam and the distance between the CCD fluorescence screen and the point where the beam intercept the sample plane is crucial in determining the precise angles of the diffracted beams. These constants are measured by fitting a Laue picture of a perfect crystal with the least square method. A special algorithm was developed for this calibration and combined into our automatic indexing program. In our measurements, a monolithic Ge crystal was used as an unstrained reference crystal and more than 40 reflections were collected to get the best fitting parameters.

## RESULTS

Here we present results of texture measurements of Al interconnects and an energy analysis of a diffracted beam from nanoindents on a Cu crystal as examples which show the potential of x-ray microbeams as a texture and strain analysis tool. A comprehensive strain analysis of Al interconnects on a memory chip is discussed in a separate paper of this proceeding[7].

Fig. 2 shows a texture map of an Al interconnect on a commercially fabricated VLSI memory chip. The interconnects were made of 0.7 μm thick film of pure Al deposited on a Si (100) surface and were covered with an amorphous glass passivating layer. The measurements were made on 2 μm wide interconnects with a 1.5 x 2 μm beam from an earlier K-B mirror

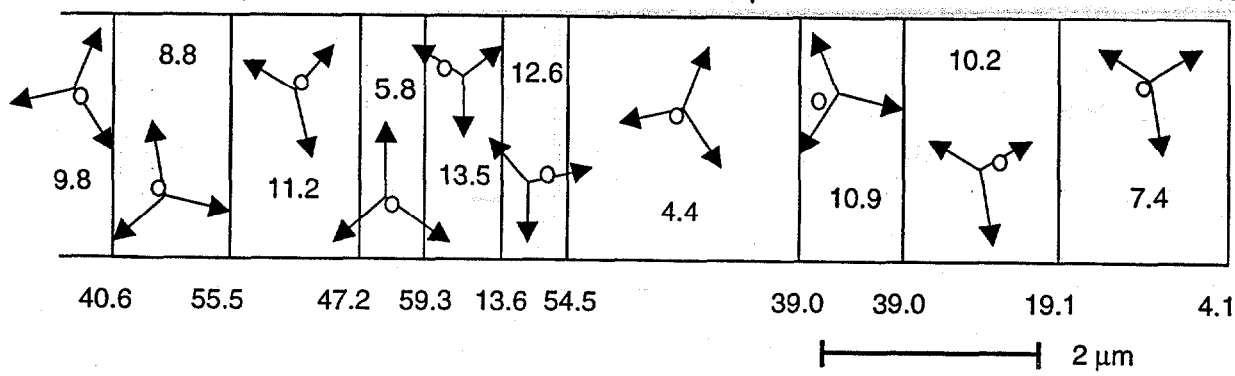


Figure2. Orientation map of grains in a 2 μm wire. The numbers are angles(°) between the surface normal and [111] directions of grains. Arrows denote the crystal axes. The circles represents (111) axes of each grain. The numbers at the bottom are rotation angles between grains. This texture map was measured with a 1.5 x 2 μm beam.

pair. All of the grains have <111> directions close to the surface normal. This agrees with the well known preferred growth of fcc metal films in the <111> direction[8,9]. The angles between the surface normal and the <111> direction of Al were in the range of ~ 3 to 14°. The orientations of the unit cells in the plane perpendicular to the <111> directon showed essentially random behavior, which is typical for high rate film growth[10]. If there were no passivating layer on top of the Al interconnects, electron backscatter diffraction would provide similar information, but would not provide strain analysis as we report in a separate paper of this proceedings[7].

As another study, Fig. 3 shows white beam Laue images taken near a nanoindent on a Cu single crystal. The indent was made with a pyramidal tip as shown in Fig. 3 on a <111> surface of a Cu single crystal. The Laue images were taken at various locations within the pyramidal crater made by the nanoindenter. Pictures taken near the centers of three faces of the pyramidal indent show strong streaking of the <111> Cu reflection toward the indenter surface normal vectors. The energy scan with a monochromatic beam shown in Fig. 4 reveals that these streaks are as wide as 500 eV and span more than 20° in angle, but the dilatational strain is quite small according to the measured d-spacings. The slight residual compression is not much larger than the present accuracy of the absolute d-spacing ($\sim 2\times10^{-4}$). In any case, the almost constant relative d-spacings indicate that the distortions are mostly plastic subgrain rotations. The absolute accuracy of the d-spacing will be improved as measurement and analysis techniques are refined.

These two examples show that x-ray microdiffraction is a unique tool that can provide new information like texture, orientation, and strain on a micron scale. This type of information will form a guide to a better understanding of the physical properties of thin film polycrystalline samples, which is needed to improve reliability in electronic devices. As shown by Wang et al.[11], the nondestructive, penetrating nature of x-rays makes it possible to monitor changes of texture and strain in real time as well to study the evolution of mesoscale

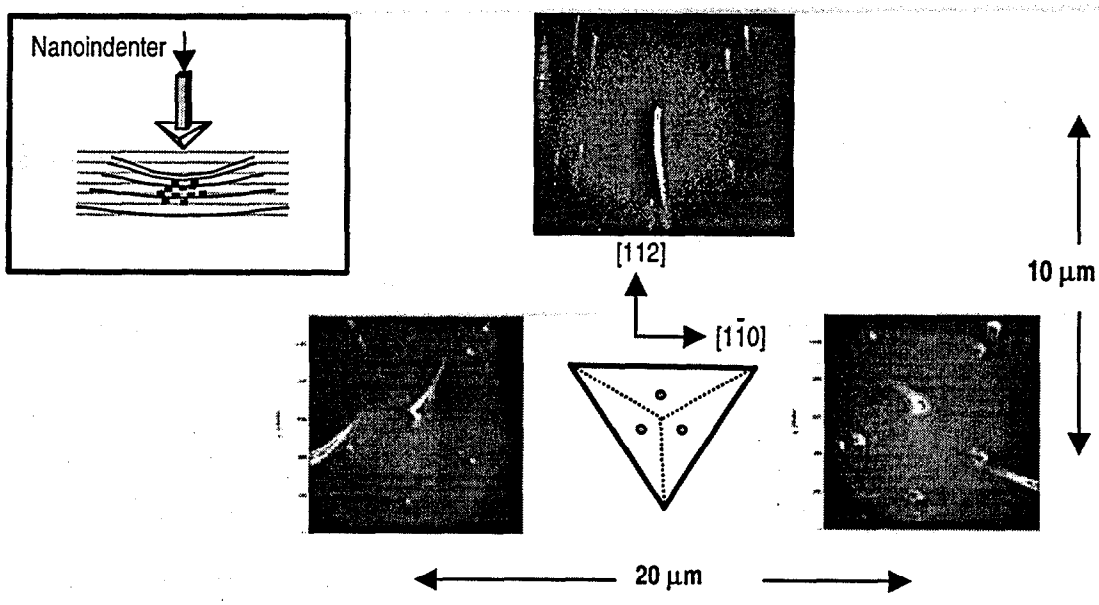


Figure 3. White beam Laue images of a nanoindented Cu single crystal. Pictures were taken at various locations in the pyramidal crater created by the nanoindenter. Approximate locations are marked as green dots in the drawing in the middle.

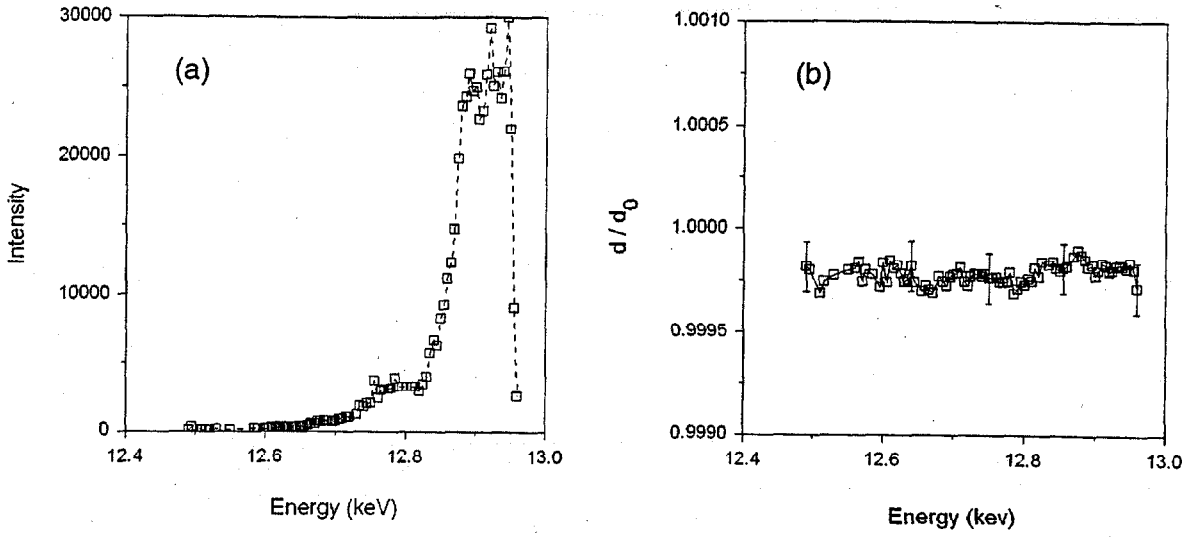


Fig. 4. Energy analysis of the [333] reflection from nanoindents on Cu. (a) Intensity vs. Energy. (b) Change in d-spacing vs. Energy.

structures due to electro-migration.

## ACKNOWLEDGEMENTS

Research sponsored by the Division of Material Sciences, U.S. Department of Energy under contract DE-AC05-96OR22464 with Lockheed Martin Energy Research Corporation. We wish to gratefully acknowledge the help of Rheinhardt Pahl, John Z. Tischler and Paul Zchack in the micromonochromator fabrication and testing. We also thank MHATT-CAT staff members, Eric Dufrene and Ernest Williams for helping in setting up our experiment. The nanoindendation on the Cu crystal was done with the help of George Pharr.

## REFERENCES

1. 1. D. J. Dingley and V. Randle, J. Mater. Sci. **27**, p. 4545 (1992).
2. Jin-Seok Chung and Gene E. Ice, Mat. Res. Soc. Symp. proc., Vol. 524 (1998).
3. Jin-Seok Chung and Gene E. Ice, submitted to J. Appl. Phys., 1999.
4. W. R. Busing and H. A. Levy, Acta Cryst. **22**, p. 457 (1967).
5. I. C. Noyan, J. B. Cohen, *Residual Stress*, Springer-Verlag, New York, NY, 1987, p.20.
6. Gene Ice, Bernie Riemer, and Ali Khounsary, SPIE proc., Vol. 2856, p. 226 (1996).
7. N. Tamura, J.-S. Chung, G. E. Ice, B. C. Larson, J. D. Budai, J. Z. Tischler, M. Yoon, E. L. Williams, W. P. Lowe, Mat. Res. Soc. Symp. proc., Vol. 563 (1999).
8. J. M. Blocher, Jr., J. Vac. Sci. Technol. **11**, p. 680 (1974).
9. R. Hergt and H. Pfeiffer, Phys. Stat. Sol. (a) **92,** p. K89 (1985).
10. J. A. Thornton, Ann. Rev. Mater. Sci. **7**, p. 239 (1977).
11. P.C. Wang, G.S. Cargill III, I.C. Noyan, and C.-K. Hu, Appl. Physics Lett. **72**, pp. 1296-1299 (1998).